CHINESE OPTICS LETTERS

Vol. 21, No. 11 | November 2023

Generation and application of structured beams based on double-phase holograms [Invited]

Erse Jia (贾而穡), Chen Xie (谢 辰)*, Yue Yang (杨 悦), and Minglie Hu (胡明列)

Ultrafast Laser Laboratory, Key Laboratory of Opto-electronic Information Technical Science of Ministry of Education, School of Precision Instruments and Opto-electronics Engineering, Tianjin University, Tianjin 300072, China

*Corresponding author: xie_chen@tju.edu.cn

Received July 31, 2023 | Accepted October 11, 2023 | Posted Online November 9, 2023

The manipulation of structured light beams requires simultaneous spatial modulation of amplitude and phase. Based on the double-phase holography (DPH) algorithm, we demonstrate an efficient reconstruction of Bessel beams with arbitrary on-axis intensity. Also, the off-axis DPH method enables more than doubled laser energy utilization compared with the widely-used off-axis phase wrapping modulation method. The DPH algorithm is also used in two-photon polymerization to enable the rapid fabrication of microtube arrays, ortho-hexagonal scaffolds, and 2D patterned microstructures. This work gives experimental proof to show the powerful feasibility of the DPH method in constructing economic adaptive laser processing systems.

Keywords: double-phase; hologram; structured beam; two-photon polymerization.
DOI: 10.3788/COL202321.110002

1. Introduction

Since Gabor introduced the concept of holography in 1948[1], hologram technology has also evolved with the development of the computer technology and the display devices. At present, the hologram can be directly generated as the computer-generated hologram (CGH)[2–4] and spatial light modulators (SLMs) have become the main key device for reconstructing the CGH due to their digital and dynamic encoding capabilities to allow modulating phase and amplitude in various configurations[5–7]. In particular, the generation of predefined structured light beams based on SLMs provides great flexibility for building adaptive optics systems in additive or subtractive manufacturing[8–11], optical micromanipulation[12], and super-resolution imaging[13].

Among the various structured lights, Bessel beams[8,9] and Airy beams[14] have been intensively investigated in the past decades. Various solutions have been developed to control the customizable 3D intensity profiles[15–18], and one of the common key factors lies in modulating the complex 2D wavefront in the initial plane. Driven by the demands for low-cost adaptive optics systems, complex amplitude modulation with a single phase-only SLM has been reported with different approaches in direct space. The most widely-used "off-axis CGH" method reconstructs the complex field in the first-order diffraction with the amplitude controlled by the phase wrapping modulation[19]. However, the primary limiting factor for this method is the relatively low laser energy utilization with a typical efficiency ~10%[15,17]. A possible scheme for high energy utilization in complex amplitude modulation is the double-phase hologram (DPH)[20,21] by superposing two phase-only profiles, which has been originally developed for advanced display technology[22].

In this paper, we demonstrate the powerful feasibility of the DPH algorithm in shaping structured light beams and multi-photon parallel additive manufacturing with a single phase-only SLM. First, we reconstruct the Bessel and Airy beams with the DPH patterns. The reliability of this algorithm is confirmed by the excellent agreement between the experimental and numerical results. Furthermore, we also demonstrate the feasibility of the DPH-based flexible control of the 3D structured beams. Three Bessel beams are well constructed with linearly increasing, linearly decreasing, and uniform on-axis intensity profiles. Additionally, DPH-based beam shaping also realizes more than doubled the laser energy utilization rate compared with the well-known "off-axis CGH" approach. These advantages further allow highly efficient DPH-assisted two-photon polymerizations (2PPs). Various structured beams are generated accordingly to enhance the fabrication efficiencies of microstructures compared with the 3D point-by-point direct laser writing (DLW) technique. Single scan molding of microstructures (microtube arrays and ortho-hexagonal scaffolds) instrumented with Bessel beams and patterning exposure of different shapes were accomplished using different modulation modes of the DPH.

2. Methods

A target field $E_{\text{tar}}(x,y)$ propagating in free space can be described by its amplitude $A_{\text{tar}}(x,y)$ and its phase $\Phi_{\text{tar}}(x,y)$ as $E_{\text{tar}}(x,y) = A_{\text{tar}}(x,y) \cdot \exp[i\Phi_{\text{tar}}(x,y)]$. In the DPH algorithm, $E(x,y)$ is expressed as the sum of two coherent fields with arbitrary amplitude A_0,

$$E(x,y) = E_1 + E_2, \tag{1}$$

where

$$E = A_0 \cos\left(\frac{\Delta\Phi}{2}\right) \cdot \exp\left[i\frac{\Phi_1(x,y) + \Phi_2(x,y)}{2}\right]. \tag{2}$$

Here, the target phase Φ_{tar} needs to match the wavelength and numerical aperture of the setup and is represented by the sum of two phases Φ_1 and Φ_2. The phase difference is written as $\Delta\Phi = \Phi_2 - \Phi_1$. Since the target amplitude A_{tar} is proportional to $\cos(\Delta\Phi/2)$, $\Delta\Phi$ can be easily obtained from the arbitrary amplitude A_0 and the predefined amplitude A_{tar}. In this way, Φ_1 and Φ_2 can be calculated from

$$\begin{aligned}\Phi_1(x,y) &= \frac{2\Phi_{\text{tar}} - \Delta\Phi}{2} = \Phi_{\text{tar}} - \arccos\,\Lambda,\\ \Phi_2(x,y) &= \frac{2\Phi_{\text{tar}} + \Delta\Phi}{2} = \Phi_{\text{tar}} + \arccos\,\Lambda,\end{aligned} \tag{3}$$

where $\Lambda = A_{\text{tar}}/A_0$. Note that $0 \le \Lambda \le 1$, and when $\Lambda = 1$, there is $\Phi_1(x,y) = \Phi_2(x,y) = \Phi_{\text{tar}}$.

To implement the above algorithm in experiments, the encoding technique in the pixelated SLM is also critical. Mendoza-Yero *et al.*[23] proposed a single-pixel-based checkerboard pattern to encode two phase maps Φ_1 and Φ_2 into a single hologram. In this method, two checkerboard patterns, represented as $M_1(x,y)$ and $M_2(x,y)$, with pixelated complementary transmittance $M_1(x,y) + M_2(x,y) = 1$ can be described by the following expressions:

$$\begin{aligned}M_1(i,j) &= \begin{cases} 1 & i+j \text{ is even} \\ 0 & \text{else} \end{cases},\\ M_2(i,j) &= \begin{cases} 1 & i+j \text{ is odd} \\ 0 & \text{else} \end{cases}.\end{aligned} \tag{4}$$

Here, i and j are the pixel indices along the x- and y-directions on the SLM. Hence, the DPH can be encoded as

$$\text{Phase}(x,y) = \Phi_1(x,y)M_1(x,y) + \Phi_2(x,y)M_2(x,y). \tag{5}$$

Since this sampling method allows a rather efficient arrangement of DPH in a single SLM, we adapt this encoding approach to the procedure, as shown in Fig. 1, to implement the double-phase-based complex wave-front shaping.

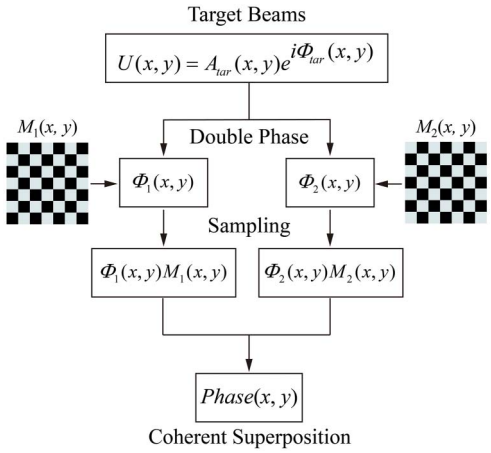

Fig. 1. Flowchart of beam shaping based on double-phase checkerboard sampling.

3. Experiments and Results

3.1. Setup

The setup for beam shaping is shown in Fig. 2. The laser source is a homemade femtosecond laser amplification system, enabling 90-fs transform-limited laser pulse centered at 1038 nm output at 1-MHz repetition rate. After expansion (L_1 and L_2), the laser beam illuminates a phase-only SLM (Holoeye PLUTO, 1920 × 1080 pixels, pixel pitch 8 μm) with adjustable intensity by the neutral density (ND) filter. The lens L_3 ($f = 1$ m) and the microscope objective MO_1 (Olympus 20×, NA = 0.4 or 50×, NA = 0.8) form a telescope system with a demagnification factor of ∼111 or ∼278. Another set of microscope objectives (MO_2, Olympus 50×, NA = 0.8) and lens L_4 ($f = 200$ mm), together with a CCD sensor, make up the imaging system to capture the intensity profiles at each z position along the beam propagation. Since most of the applications utilize the linearly polarized beam, we limited our work in the scalar optics.

Figure 2(c) schematically shows the encoded double-phase pattern loaded on the SLM. To fully utilize the space-bandwidth product of the SLM, each cell in the checkerboard grating pattern contains four SLM pixels, as shown in the inset. In addition, by adding a blazed grating phase to the double-phase pattern[24], the limited apertures in the setup can automatically eliminate the zeroth-order noise introduced by the pixelated SLM.

3.2. DPH-based structured beams generation

To test the DPH-based encoding procedure in Fig. 1, we first utilize the double-phase method to generate the well-known non-diffracting Bessel beam[25] and the Airy beam[26]. The target phase for the Bessel beam is $\Phi_{\text{tar}}(x,y) = -2\pi\rho/\rho_0$ with ρ_0 set as 0.5 mm. Additionally, we also measure the power converted into the Bessel beams with various uniformly attenuated target amplitudes $A_{\text{tar}}(x,y)$. In this test, a 10-mW laser power is incident on the SLM. The measured power efficiency is plotted in Fig. 3 with the parameter $\Lambda = A_{\text{tar}}/A_0$ defined in Eq. (3). As

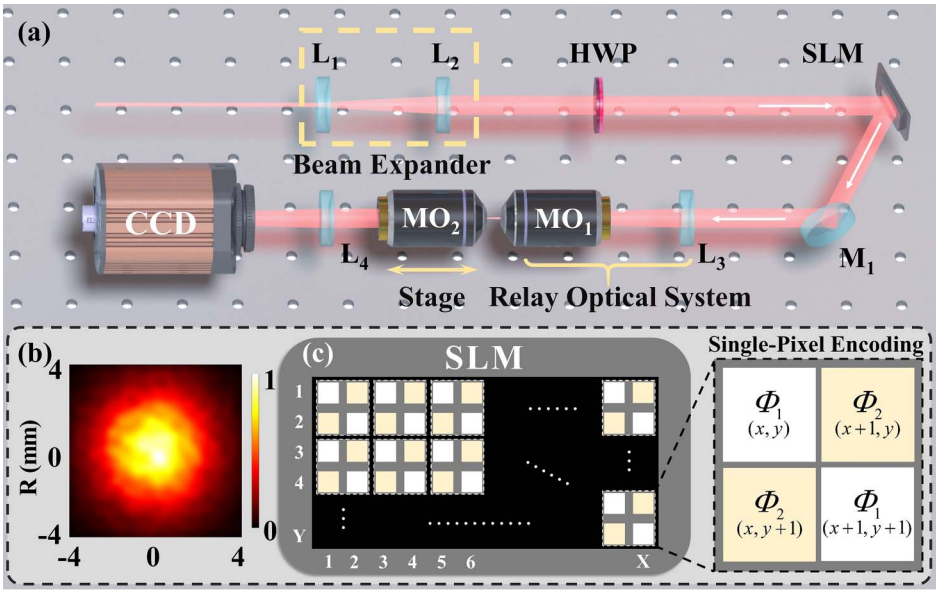

Fig. 2. Complex amplitude beam shaping. (a) Schematic of the experimental setup. HWP, half-wave plate; SLM, spatial light modulator; M1, mirror; L_1, L_2, L_3, and L_4, lenses; MO_1 and MO_2, microscope objectives. (b) Intensity profile of the incident beam on the SLM captured with the CCD in the setup. (c) Schematic of the double-phase distribution loaded on the SLM after checkerboard sampling.

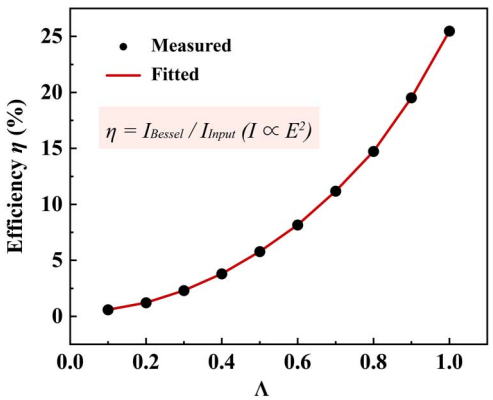

Fig. 3. Beam shaping efficiency η versus parameter Λ.

presented in Fig. 3, the efficiency curve can be well fitted by the expected parabolic function, as inferred from Eq. (3). As Λ approaches 1, the Bessel beam is reproduced with an efficiency close to 25%.

The input- and the target-amplitudes of the Bessel beams are shown in the first row of Fig. 4(a), where the white solid line outlines the intensity profiles across the maxima. The corresponding double-phases $\Phi_1(x, y)$ and $\Phi_2(x, y)$ are encoded in the checkerboard pattern, as shown in Fig. 4(a). Figure 4(b) presents the longitudinal intensity profiles of the Bessel beams after the objective MO_1. Numerical simulations based on the angular spectrum method are in excellent agreement with the experimental results, with the main lobe extended in the 250-μm range.

To further validate the wave-front reconstruction capability of the DPH-based algorithm, we generate two Airy beams along different trajectories. Table 1 lists the parameters of the self-accelerating curves.

The target phases of the curved beams can be pre-determined by the method in Ref. [27]. The corresponding phase masks after checkerboard sampling are shown in Figs. 5(a) and 5(d). Numerical simulations are also performed before implementing the experiments as shown in Figs. 5(b) and 5(e). In both simulation and experiments, the laterally accelerated trajectories of the main lobe closely fit the pre-designed curves as shown with the white dashed lines. The central intensity peaks exhibit the qualitative features of the primary Airy lobe in the selected cross sections, as shown in Fig. 5. Tiny deviations from the ideal beams occur in the transverse intensity profile at the end of the propagation. We attribute this feature to the inherent limitations of the experimental setup, such as the small aperture in the microscope objective and/or the dimensions of the SLM. In general, the high agreement between the experimental results and the simulations indicates that the pixel crosstalk inherent in the DPH algorithm does not adversely affect the reconstruction of the shaped beam.

3.3. DPH-based intensity control of non-diffracting beams

Complex amplitude shaping via a single phase-only hologram in direct space has been reported with different approaches. The most widely used solution tweaks the amplitude in the first order by modulating the phase wrapping depth[19]. However, this "off-axis CGH" method always appears with a low energy utilization rate due to the vast majority of energy diffracted into the undesired zeroth order. For instance, with this approach, only ~10% input energy can be converted into the Bessel beams with various on-axis intensity profiles along the propagation[15].

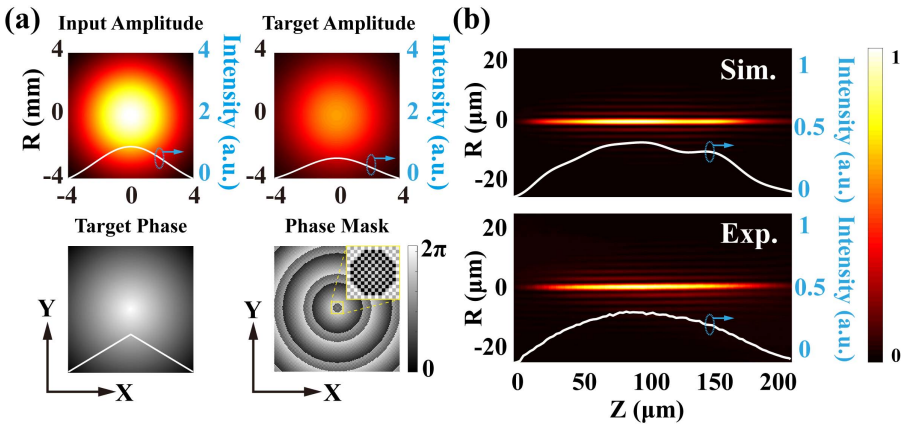

Fig. 4. Bessel beam generation based on DPH algorithm. (a) Top, input and target amplitude profiles. Bottom, target phase and the corresponding DPH map. (b) Longitudinal intensity profiles with white solid lines as the on-axis intensity distributions of the main lobe along propagation. Top, numerical simulations. Bottom, experimental results.

Table 1. Self-Accelerating Trajectories of the Airy Beams.

Trajectory	Formulas and Parameters
Hook	$c(z) = a(z - z_0) + \frac{b}{z - z_0} + c$, $a = 0.0015$ μm, $b = 4.33 \times 10^9$ μm, $c = -3.5$ mm, $z_0 = 1 \times 10^3$ mm
Parabolic	$c(z) = a(z - z_0)^2 + b$, $a = 1 \times 10^{-9}$ μm, $b = 0.92$ mm, $z_0 = 1.4 \times 10^3$ mm

For comparison, we engineer the on-axis amplitude of the Bessel beam based on both the DPH method and the widely used off-axis phase wrapping modulation method. Three Bessel beams with linearly increasing, linearly decreasing, and uniform on-axis intensity profiles are designed in a similar principle to Ref. [15]. Figure 6 shows the simulated and experimental results of the DPH-shaped beams. The first row of the figure presents the input Gaussian amplitudes and the target amplitudes. Under all the preset conditions, the reconstructed on-axis intensity profiles agree well with the targets and the numerical results, as shown in Fig. 6. In Fig. 7, we further compare the efficiencies of two complex amplitude modulation methods at the same laser power incident on the SLM. Despite the efficiency fluctuation due to the complicated target on-axis intensity profiles[15], the DPH-based algorithm enables a more than doubled energy utilization rate in the engineered Bessel beams compared with the phase-wrapping modulation method.

4. Applications

Among the many solutions to additive manufacturing, femtosecond 2PPs have been widely adopted in key device fabrications in various applications[28,29], such as micro-optics, on-chip optical interconnects, and biological architectures. However, traditional voxel-by-voxel laser writing strategies are usually limited within the laboratory research and prototyping, constrained by the inefficient 2PP material processing. The limited two-photon absorption cross section further restricts the expansion of 2PP for wide-area fabrication. Recent studies have shown that on-demand parallel 2PP lithography printing based on complex amplitude modulation can provide higher fabrication efficiency[30-33]. This strategy does not require scanning of the focal point but rather a one-step exposure to achieve high-speed processing. In this section, we demonstrate the parallel direct writing capability of the DPH algorithm-assisted 2PP, and the higher energy utilization reduces the laser performance requirements of the laser direct writing technology.

Figure 8(a) shows a schematic diagram of the experimental setup for femtosecond laser 2PP. The laser source is the same as in Fig. 3, and a BBO crystal is inserted to generate the second-harmonic (SH) wave for the 2PP fabricating process. A telescope consisting of a lens ($f = 1$ m) and a microscope objective (Olympus 50×, NA = 0.8) shrinks the modulated waves into microscaled patterns and re-images it inside the photoresist. In the 2PP experiment, the sample is prepared by spin coating the negative photoresist (MicroChem SU-8 2035) onto standard slide substrates at a speed of 1600 r/min. Soft baking was performed on a hot plate for 90 min at 65 °C.

DPH algorithm-assisted 2PP employs two different parallel direct-writing modes. One of them is dominated by complex amplitude modulation, and Figs. 8(b1)–8(b3) demonstrate the rapid fabrication of ortho-hexagonal scaffolds and microtube arrays with a height of 60 μm based on the Bessel beam generated by the DPH algorithm. The main lobe of the Bessel beam propagates across the entire photoresist layer, and the height of the microstructure is determined by the layer thickness, so the time consumption is the same no matter how high the microstructure is. The non-diffractive nature of the Bessel beam simplifies the point-by-point 3D-DLW into the 2D-pattern scan, resulting in an overall manufacturing time of less than 2 minutes in comparison with the ~51 minutes with the 3D point-by-point DLW in our system. Furthermore, our scheme would enable

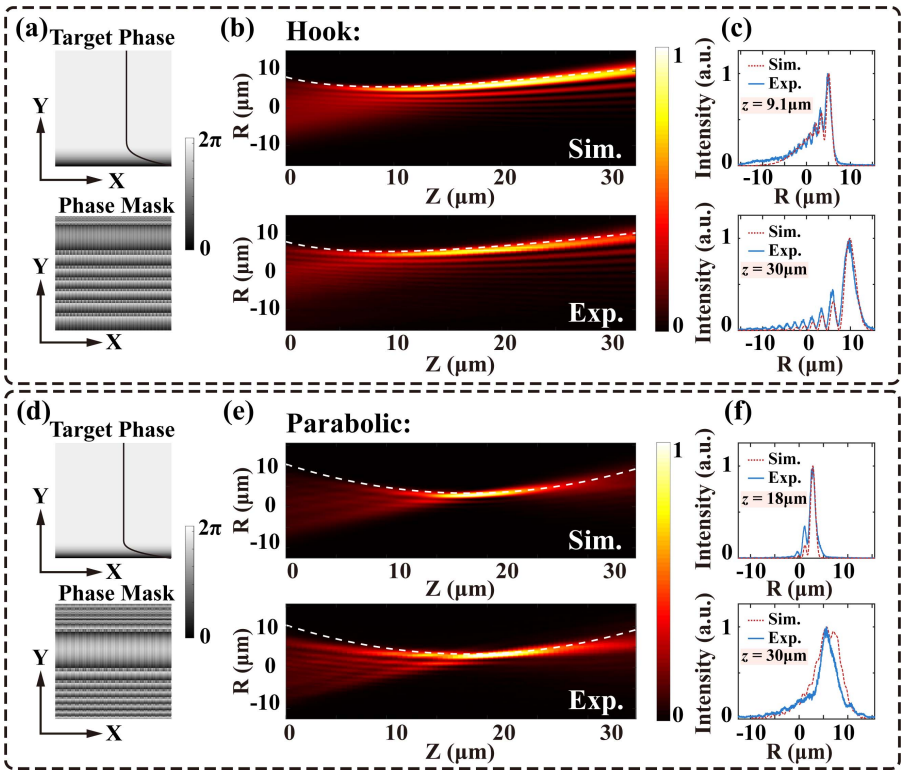

Fig. 5. Airy beam generation with DPH-based encoding method. (a), (d) Target phases and the corresponding DPH maps. (b), (e) Longitudinal intensity profiles with white dashed lines as the predefined Hook and parabolic trajectories (top, simulations; bottom, experiments). (c), (f) Intensity profiles in the selected cross sections.

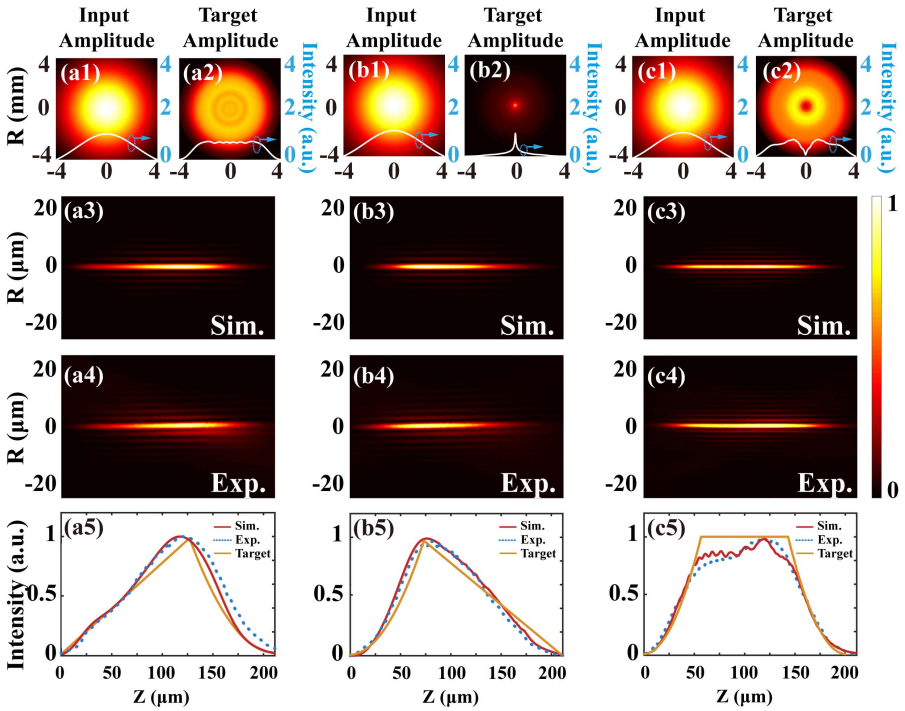

Fig. 6. DPH-based intensity control. Amplitudes profiles, simulated (Sim.) and experimental (Exp.) 2D intensity maps with three tailored on-axis intensity profiles: (a1)–(a5) linearly increasing, (b1)–(b5) linearly decreasing, and (c1)–(c5) uniform. The input and the target amplitude profiles are compared in the first row of each column.

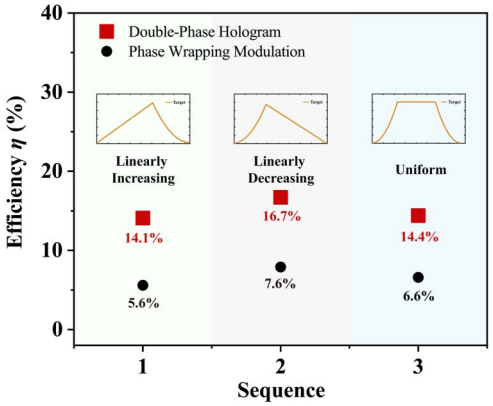

Fig. 7. Comparison of the efficiencies of the two complex amplitude modulation methods for generating Bessel beams. The insets schematically represent the corresponding target on-axis intensity profiles of each tailored Bessel beam.

higher efficiency in fabricating a taller microstructure. For example, the fabrication efficiency with the Bessel beam can be enhanced by a factor of ~50 in comparison with the point-by-point DLW method for microstructures with heights of ~100 μm.

Another parallel fabrication strategy we demonstrated is the patterned exposure dominated by the DPH-based amplitude modulation. The hexagonal, triangular, and square patterns were chosen as the target amplitude and the plane wave as the target phase. After the double-phase computation and sampling, the intensity profiles at the working plane of the microscope objective (MO in Fig. 8) are generated with a high degree of agreement with the desired patterns. Unlike the previous parallel strategy, patterned exposures require only z-direction scanning during execution, and the created height is controllable. The SEM photos of fabricated structures with a height of 6 μm are shown in Figs. 8(c)–8(e).

5. Conclusion

In this paper, we demonstrate the feasibility of utilizing a DPH algorithm for diffraction-free beam generation and control. For beam generation, we use the DPH algorithm combined with spatial sampling of complementary binary gratings to generate Bessel beams and Airy beams with customizable self-accelerating trajectories with high quality. The good agreement between experimental and numerical results confirms the weak effect of the pixel crosstalk in the DPH-based method on beam shaping. On this basis, Bessel beams with linearly increasing, linearly decreasing, and uniform on-axis intensity profiles are reconstructed by complex amplitude modulation. The energy conversion rates of the beams are 14.1%, 16.7%, and 14.4%, respectively, more than twice that of the phase wrapping modulation method. Improved energy utilization allows less dependence on the light source performance for a variety of applications, particularly in building cost-effective laser fabricating systems. Further, we demonstrate the micro-fabrications with the DPH-based femtosecond 2PP technology in two modes. In the exemplary fabrications of the microstructure arrays with heights of 60 μm, our scheme with 2D scans of the Bessel beam consumes only ~4% of the time in the traditional 3D point-by-point DLW method. Moreover, parallel direct writings have also been demonstrated in fabricating a microstructure with highly controllable light patterns shaped by the DPH-based method. We expect the reliability, high efficiency, and high energy utilization of the DPH-based method would further accelerate and facilitate the commercialization

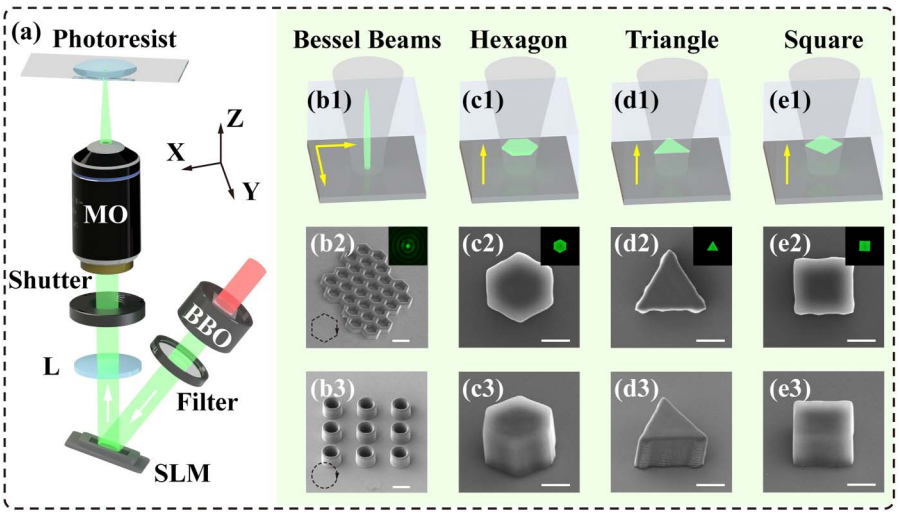

Fig. 8. DPH-assisted 2PP. (a) Schematic of the 2PP setup. The first row of (b1)–(e1) shows the relative position between the photoresist and the structured light beams. The second row, (b2)–(e2), and the third row, (b3)–(e3), show the SEM photos of the resulting microstructure fabricated via 2PP with the insets presenting the transverse intensity profiles in the experiments. Scaling bars in (b2) and (b3) represent 50 μm and others represent 5 μm.

of the hologram-based fabrications in various fields, such as anti-reflective microstructures, photonic crystal filters, and nano-pillars.

Acknowledgement

This work was supported by the National Natural Science Foundation of China (Nos. 62275191, 61605142, and 61827821), the Tianjin Research Program of Application Foundation and Advanced Technology of China (No. 17JCJQJC43500), and the Shanghai Institute of Optics and Fine Mechanics, Chinese Academy of Sciences (Open Fund of the State Key Laboratory of High Field Laser Physics).

References

1. D. Gabor, "A new microscopic principle," Nature **161**, 777 (1948).
2. L. B. Lesem, P. M. Hirsch, and J. A. Jordan, "The kinoform: a new wavefront reconstruction device," IBM J. Res. Dev. **13**, 150 (1969).
3. D. Pi, J. Liu, and Y. Wang, "Review of computer-generated hologram algorithms for color dynamic holographic three-dimensional display," Light Sci. Appl. **11**, 231 (2022).
4. P. Genevet and F. Capasso, "Holographic optical metasurfaces: a review of current progress," Rep. Prog. Phys. **78**, 024401 (2015).
5. K. Yin, E.-L. Hsiang, J. Zou, Y. Li, Z. Yang, Q. Yang, P.-C. Lai, C.-L. Lin, and S.-T. Wu, "Advanced liquid crystal devices for augmented reality and virtual reality displays: principles and applications," Light Sci. Appl. **11**, 161 (2022).
6. Z. Zhang, Z. You, and D. Chu, "Fundamentals of phase-only liquid crystal on silicon (LCOS) devices," Light Sci. Appl. **3**, e213 (2014).
7. M. P. Edgar, G. M. Gibson, and M. J. Padgett, "Principles and prospects for single-pixel imaging," Nat. Photonics **13**, 13 (2019).
8. R. Stoian, M. K. Bhuyan, G. Zhang, G. Cheng, R. Meyer, and F. Courvoisier, "Ultrafast Bessel beams: advanced tools for laser materials processing," Adv. Opt. Technol. **7**, 165 (2018).
9. M. Duocastella and C. B. Arnold, "Bessel and annular beams for materials processing," Laser Photonics Rev. **6**, 607 (2012).
10. L. Yang, A. El-Tamer, U. Hinze, J. Li, Y. Hu, W. Huang, J. Chu, and B. N. Chichkov, "Two-photon polymerization of cylinder microstructures by femtosecond Bessel beams," Appl. Phys. Lett. **105**, 041110 (2014).
11. X. Liu, R. Clady, D. Grojo, O. Utéza, and N. Sanner, "Engraving depth-controlled nanohole arrays on fused silica by direct short-pulse laser ablation," Adv. Mater. Interfaces **10**, 2202189 (2023).
12. D. McGloin, V. Garcés-Chávez, and K. Dholakia, "Interfering Bessel beams for optical micromanipulation," Opt. Lett. **28**, 657 (2003).
13. W. Yu, Z. Ji, D. Dong, X. Yang, Y. Xiao, Q. Gong, P. Xi, and K. Shi, "Super-resolution deep imaging with hollow Bessel beam STED microscopy," Laser Photonics Rev. **10**, 147 (2016).
14. N. K. Efremidis, Z. Chen, M. Segev, and D. N. Christodoulides, "Airy beams and accelerating waves: an overview of recent advances," Optica **6**, 686 (2019).
15. I. Ouadghiri-Idrissi, R. Giust, L. Froehly, M. Jacquot, L. Furfaro, J. M. Dudley, and F. Courvoisier, "Arbitrary shaping of on-axis amplitude of femtosecond Bessel beams with a single phase-only spatial light modulator," Opt. Express **24**, 11495 (2016).
16. M. Mazilu, D. J. Stevenson, F. Gunn-Moore, and K. Dholakia, "Light beats the spread: "non-diffracting" beams," Laser Photonics Rev. **4**, 529 (2010).
17. T. Čižmár and K. Dholakia, "Tunable Bessel light modes: engineering the axial propagation," Opt. Express **17**, 15558 (2009).
18. M. Goutsoulas and N. K. Efremidis, "Precise amplitude, trajectory, and beam-width control of accelerating and abruptly autofocusing beams," Phys. Rev. A **97**, 063831 (2018).
19. J. A. Davis, D. M. Cottrell, J. Campos, M. J. Yzuel, and I. Moreno, "Encoding amplitude information onto phase-only filters," Appl. Opt. **38**, 5004 (1999).
20. C. K. Hsueh and A. A. Sawchuk, "Computer-generated double-phase holograms," Appl. Opt. **17**, 3874 (1978).
21. W. Liu, Y. Lu, L. Gong, X. Chu, G. Xue, Y. Ren, M. Zhong, Z. Wang, J. Zhou, and Y. Li, "Dynamic enhancement of autofocusing property for symmetric Airy beam with exponential amplitude modulation," J. Opt. **18**, 075301 (2016).
22. X. Sui, Z. He, G. Jin, and L. Cao, "Spectral-envelope modulated double-phase method for computer-generated holography," Opt. Express **30**, 30552 (2022).
23. O. Mendoza-Yero, G. Mínguez-Vega, and J. Lancis, "Encoding complex fields by using a phase-only optical element," Opt. Lett. **39**, 1740 (2014).
24. Y. Qi, C. Chang, and J. Xia, "Speckleless holographic display by complex modulation based on double-phase method," Opt. Express **24**, 30368 (2016).
25. J. Durnin, J. J. Miceli, and J. H. Eberly, "Diffraction-free beams," Phys. Rev. Lett. **58**, 1499 (1987).
26. G. A. Siviloglou and D. N. Christodoulides, "Accelerating finite energy Airy beams," Opt. Lett. **32**, 979 (2007).
27. L. Froehly, F. Courvoisier, A. Mathis, M. Jacquot, L. Furfaro, R. Giust, P. A. Lacourt, and J. M. Dudley, "Arbitrary accelerating micron-scale caustic beams in two and three dimensions," Opt. Express **19**, 16455 (2011).
28. S. Kawata, H. Sun, T. Tanaka, and K. Takada, "Finer features for functional microdevices," Nature **412**, 697 (2001).
29. T. Frenzel, M. Kadic, and M. Wegener, "Three-dimensional mechanical metamaterials with a twist," Science **358**, 1072 (2017).
30. C. Zhang, Y. Hu, W. Du, P. Wu, S. Rao, Z. Cai, Z. Lao, B. Xu, J. Ni, J. Li, G. Zhao, D. Wu, J. Chu, and K. Sugioka, "Optimized holographic femtosecond laser patterning method towards rapid integration of high-quality functional devices in microchannels," Sci. Rep. **6**, 33281 (2016).
31. S. K. Saha, D. Wang, V. H. Nguyen, Y. Chang, J. S. Oakdale, and S.-C. Chen, "Scalable submicrometer additive manufacturing," Science **366**, 105 (2019).
32. H. Cheng, P. Golvari, C. Xia, M. Sun, M. Zhang, S. M. Kuebler, and X. Yu, "High-throughput microfabrication of axially tunable helices," Photonics Res. **10**, 303 (2022).
33. A. Balena, M. Bianco, F. Pisanello, and M. De Vittorio, "Recent advances on high-speed and holographic two-photon direct laser writing," Adv. Funct. Mater. **33**, 2211773 (2023).